

This work was written as part of one of the author's official duties as an Employee of the United States Government and is therefore a work of the United States Government. In accordance with 17 U.S.C. 105, no copyright protection is available for such works under U.S. Law.

Public Domain Mark 1.0

<https://creativecommons.org/publicdomain/mark/1.0/>

Access to this work was provided by the University of Maryland, Baltimore County (UMBC) ScholarWorks@UMBC digital repository on the Maryland Shared Open Access (MD-SOAR) platform.

Please provide feedback

Please support the ScholarWorks@UMBC repository by emailing scholarworks-group@umbc.edu and telling us what having access to this work means to you and why it's important to you. Thank you.

Nonmonotonic Dependence of Auger Recombination Rate on Shell Thickness for CdSe/CdS Core/Shell Nanoplatelets

Matthew Pelton,^{*,†,‡,§} Jordan J. Andrews,[§] Igor Fedin,^{||} Dmitri V. Talapin,^{‡,||} Haixu Leng,[†] and Stephen K. O’Leary[§]

[†]Department of Physics, University of Maryland, Baltimore County, Baltimore, Maryland 21250, United States

[‡]Center for Nanoscale Materials, Argonne National Laboratory, Argonne, Illinois 60439, United States

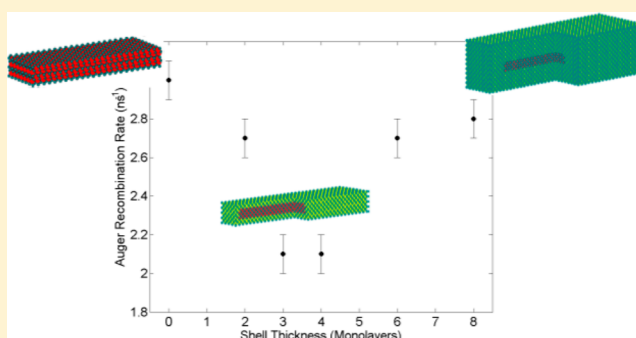
[§]School of Engineering, The University of British Columbia, Kelowna, British Columbia V1V 1V7, Canada

^{||}Department of Chemistry and James Franck Institute, University of Chicago, Chicago, Illinois 60637, United States

Supporting Information

ABSTRACT: Nonradiative Auger recombination limits the efficiency with which colloidal semiconductor nanocrystals can emit light when they are subjected to strong excitation, with important implications for the application of the nanocrystals in light-emitting diodes and lasers. This has motivated attempts to engineer the structure of the nanocrystals to minimize Auger rates. Here, we study Auger recombination rates in CdSe/CdS core/shell nanoplatelets, or colloidal quantum wells. Using time-resolved photoluminescence measurements, we show that the rate of biexcitonic Auger recombination has a nonmonotonic dependence on the shell thickness, initially decreasing, reaching a minimum for shells with thickness of 2–4 monolayers, and then increasing with further increases in the shell thickness. This nonmonotonic behavior has not been observed previously for biexcitonic recombination in quantum dots, most likely due to inhomogeneous broadening that is not present for the nanoplatelets.

KEYWORDS: Auger recombination, nanoplatelets, semiconductor nanocrystals, core–shell, time-resolved photoluminescence



The library of semiconductor-nanocrystal geometries that can be synthesized colloiddally has recently been expanded to include nanoplatelets (NPLs) that have thicknesses of a few monolayers (MLs) and lateral dimensions of 10–100 nm.¹ Carriers in these NPLs are confined quantum-mechanically in only one dimension, so that the NPLs have the electronic structure of quantum wells.² This electronic structure, in turn, enables new optoelectronic applications; in particular, NPLs are promising gain materials for solution-processed lasers. They have provided optical gain and amplified spontaneous emission with low excitation thresholds,^{3,4} for emission wavelengths throughout the visible spectral range.^{5,6} Lasers incorporating NPLs have operated under multiphoton excitation^{7,8} and have exhibited continuous-wave lasing at room temperature,⁹ including lasing with the lowest threshold of any room-temperature laser to date.¹⁰

The superior gain properties of NPLs as compared to spherical nanocrystals, or quantum dots (QDs), are attributable, at least in part, to relatively low rates for biexcitonic Auger recombination. This form of Auger recombination occurs when one exciton, or bound electron–hole pair, in the semiconductor recombines nonradiatively by increasing the kinetic energy of an electron or hole in a second exciton. Auger recombination rates in QDs are high, because carrier confinement and the

absence of dielectric screening lead to strong carrier–carrier interactions in the nanocrystals.^{11,12} If the doubly degenerate ground state of a II–VI QD is fully occupied, then, rapid Auger recombination will compete with the slow radiative recombination of excitons in these nanocrystals, leading to a low efficiency for optical emission. Since full occupation of this state is required for population inversion, QDs require high excitation powers for optical gain and lasing.^{13,14} The extensive effort that has been dedicated to reducing thresholds and demonstrating practical nanocrystal lasers has primarily involved engineering the structure of core–shell nanocrystals to suppress Auger recombination.^{15–18}

By contrast, NPLs can achieve inversion without complete occupation of the lowest-energy excitonic state, leading to lower Auger recombination rates, as compared to QDs, at exciton densities that provide gain.^{3,19,20} This has been accomplished without an explicit attempt to engineer the nanoplatelet structure to minimize Auger rates. One experimental study has probed the dependence of Auger rates in CdSe NPLs on their thicknesses and lateral dimensions.²¹ The

Received: August 2, 2017

Revised: October 4, 2017

Published: October 10, 2017

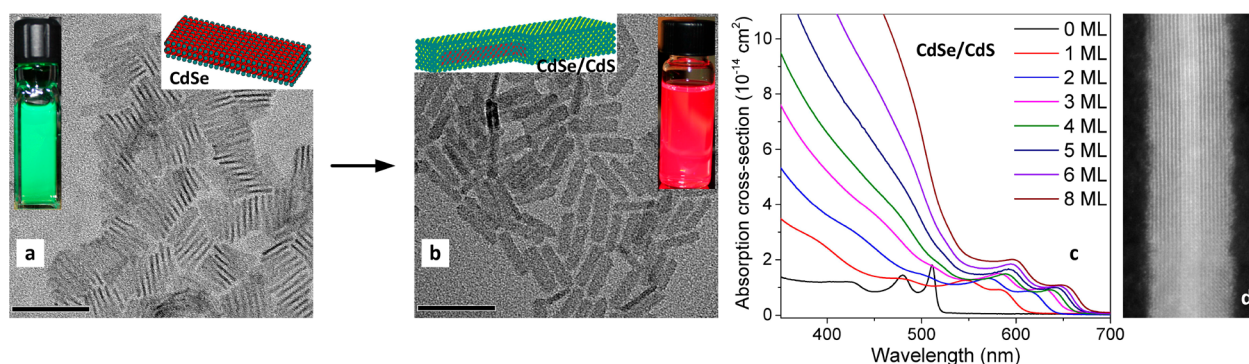


Figure 1. Growth and structure of CdSe/CdS core/shell nanoplatelets (NPLs) (a–b) Transmission electron microscope (TEM) images of (a) CdSe and (b) CdSe/CdS core/shell nanoplatelets, with CdSe thickness of 4 monolayers (ML) and CdS thickness of 3 ML. Insets: photographs of photoluminescence from dilute solutions of the NPLs and schematics of the NPLs. (c) Measured absorption spectra of CdSe/CdS core/shell NPLs with a core thickness of 4 ML and different shell thicknesses. (d) Cross-sectional dark-field TEM image of a core/shell NPL with a CdSe thickness of 4 ML and CdS thickness of 6 ML.

rates were found to scale inversely with the area of the NPLs, and with the inverse seventh power of their thickness, indicating that Auger recombination is strongly influenced by carrier confinement in these materials.

Greater control over confinement, and thus over Auger rates, should be achievable in NPL heterostructures. The Auger rates in CdSe/CdS core/shell NCs have been observed to decrease with increasing shell thickness,²² with low rates achieved for thick spherical^{23,24} or rod-shaped^{25,26} shells. Here, we investigate biexcitonic Auger recombination in CdSe/CdS core/shell NPLs.^{27,28} We find that the Auger recombination rate depends nonmonotonically on shell thickness, reaching a minimum for a thickness of 2–4 ML. This nonmonotonic behavior is qualitatively different from what has been reported in previous studies of biexcitonic Auger rates in nanocrystals and is observable because of the unique structural properties of the NPLs.

In particular, optical absorption and luminescence in NPL ensembles is nearly free of inhomogeneous broadening,²⁹ because the growth mode of NPLs leads to an ensemble that is atomically monodisperse in thickness.^{2,30} Moreover, shells can be grown on the NPLs a single atomic layer at a time by using the “colloidal atomic layer deposition” (c-ALD) method,²⁷ preserving the monodispersity in ensembles of core/shell NPLs. This means that ensemble measurements can provide the same detailed information about structure–property relationships as single-particle measurements.

We use the c-ALD method to grow a series of CdSe/CdS core/shell NPLs with two different core thicknesses and shell thicknesses from 0 ML (no shell) up to 8 ML, following published procedures.^{27,31} (Synthesis details are given in the [Supporting Information](#).) [Figure 1](#) shows representative transmission-electron-microscope (TEM) images of NPLs, as well as optical absorption spectra of a series of NPL samples with increasing shell thickness.

Exciton dynamics in these NPLs are studied by measuring time-resolved photoluminescence (PL) using a streak camera.^{19,31} (Measurement details are given in the [Supporting Information](#).) Representative results for a particular NPL sample are shown in [Figure 2a](#). The time-dependent PL intensity is proportional to the probability that an NPL emits a photon at a given time after excitation by the laser pulse. The exciton binding energy in NPLs is much greater than the room-temperature thermal energy,³² so photons are emitted by

bound excitons, rather than free electron–hole pairs. The instantaneous PL intensity is thus proportional to the average number of excitons in each NPL, $N(t)$, as a function of time after excitation. The subnanosecond decay that increases in relative magnitude and becomes faster as the pump fluence increases—that is, as the initial number of excitons produced in each nanoplatelet by the pump pulse increases—is thus an indication that the exciton population decays more rapidly when the exciton number is higher. In other words, this is a signature of a multiexciton recombination process, such as Auger recombination.

Multiexciton recombination dynamics in QDs are typically analyzed using a sum of exponential decay terms, with one term for each combination of carriers that can be involved in recombination.^{11,12} For NPLs, the large number of excitons that can be present makes this sort of analysis impractical. Instead, we obtain a universal decay curve by shifting each of the time-dependent PL-intensity traces along the time axis so that they fall on top of one another.¹⁹ The curves are arranged in descending order of pump fluence, and each curve is shifted to match the one before it. The best time shift for each curve is found by plotting the inverse of the measured intensity (which is expected to be linear in time when the dynamics are dominated by Auger recombination, as explained below) and minimizing the sum of squares between the shifted curve and the one that it is being compared to. Once this is done for all curves, universal decay dynamics are obtained, as illustrated in [Figure 2b](#).

The ability to obtain a universal decay curve indicates that the exciton recombination rate in the NPLs at a given time depends only on the exciton population at that time. In other words, exciting the sample with a high pump fluence leads to a large initial number of excitons per nanoplatelet, $N(0)$; once the exciton population decays from this initial value to a lower value, N_1 , the subsequent dynamics are the same as the dynamics obtained when the sample is excited with a lower-fluence pulse that produces N_1 excitons to begin with. We have previously observed this universal decay for CdSe NPLs;²⁰ here, we extend the measurements to pump fluences approximately 50 times lower than in our previous work. As can be seen in [Figure 2b](#), the PL decay curves for low fluences fall on top of one another without shifting along the time axis; that is, the dynamics are independent of the energy of the excitation pulse in the low-fluence regime. In this regime, any given NPL in the

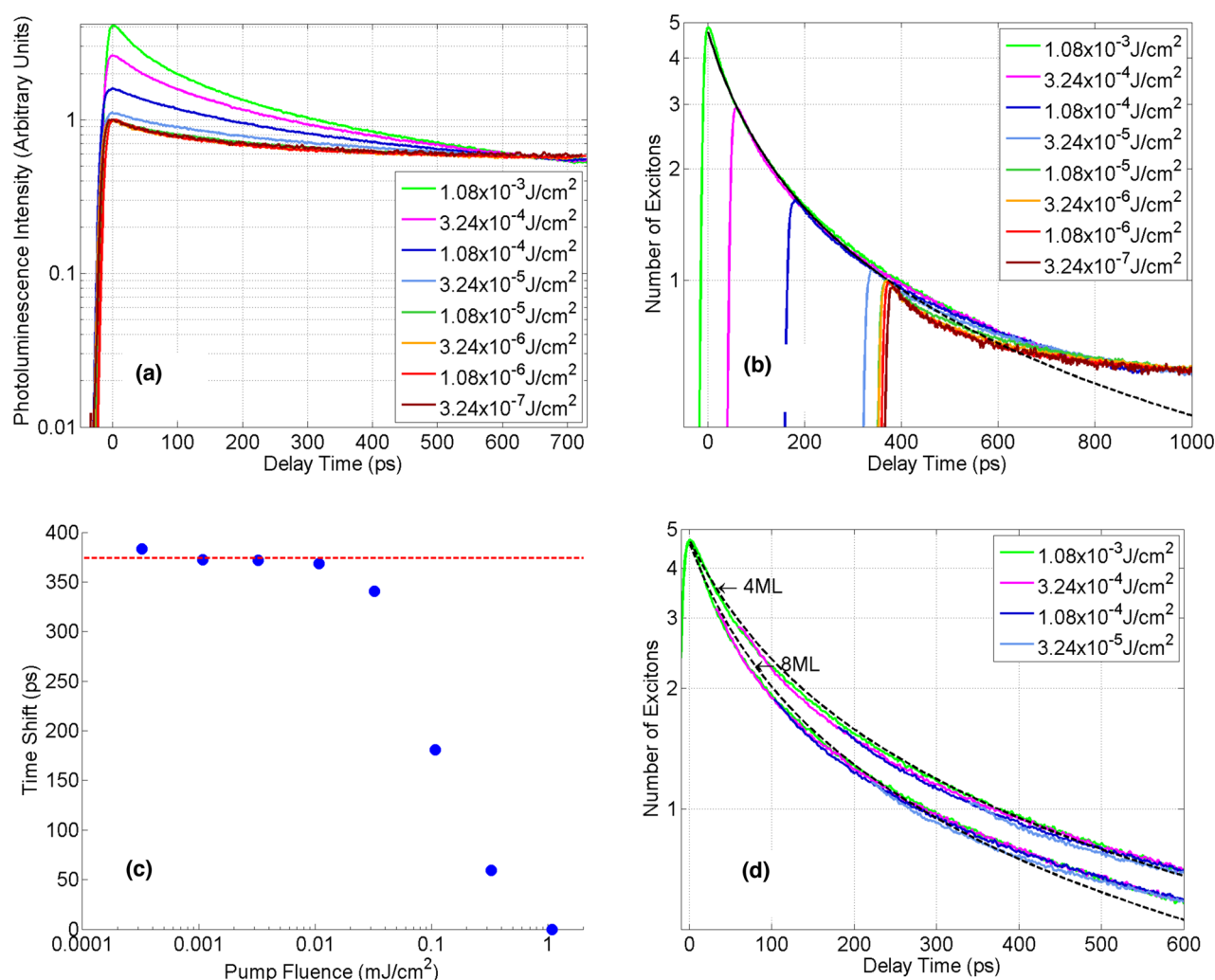


Figure 2. Time-resolved photoluminescence from CdSe/CdS core/shell nanoplatelets (NPLs) with CdSe core thickness of 4 monolayers (ML) and CdS shell thickness of 4 ML. (a) Total luminescence intensity as a function of time after pulsed excitation, for different excitation-pulse fluences. Data are normalized so that they approach the same intensity at long delay times. (b) Average number of excitons per NPL, $N(t)$, as a function of time after excitation. Results are obtained by shifting the luminescence intensities, without normalization, in time so that they fall onto the same curve. Intensities are converted to exciton number by determining the point at which the shift along the time axis becomes independent of pump fluence, corresponding to $N(t) = 1$. Also shown is a fit (black line) to the form $N(t) = N(0)/(1 + AN(0)t)$, with $N(0) = 4.7$ and $A = 2.1 \text{ ns}^{-1}$. The fitted line is solid over the regime where Auger dynamics dominates and is dashed over the regime where single-exciton dynamics dominate. (c) Amount of shift along the time axis for the photoluminescence-intensity curves as a function of pump fluence. (d) $N(t)$ as a function of time after excitation, determined by shifting and converting intensity to exciton number as in panel b, together with fits (dashed lines), for NPLs with CdSe core thickness of 4 ML and CdS shell thicknesses of 4 and 8 ML. For clarity, data are shown only for high fluences, where Auger recombination dominates the dynamics, and data for negative time delays (corresponding to the initial rise of the signals) are excluded.

ensemble is unlikely to contain more than one exciton. The NPLs that contain no excitons do not contribute to the PL signal, so the measured decay curve reflects exclusively the dynamics of NPLs that contain a single exciton. The dynamics are dominated by single-exciton recombination, with a small, subnanosecond component that is most likely due to exciton trapping.

The crossover between the low-fluence and high-fluence regimes can be seen in Figure 2c as the point where the shift is no longer constant with increasing fluence. At this crossover point, the average exciton population in the NPLs, $N(t) = 1$. We can thus use this point to calibrate the universal PL decay curve so that it corresponds directly to $N(t)$, as shown in Figure 2b. Although this method is somewhat approximate, it is similar in spirit to methods used by other authors.^{19,21} It gives a result similar to our previous method, for higher-fluence measure-

ments, based on fitting the saturation curve, but we believe this new method is more precise.²⁰ We note that the initial exciton population is smaller than what would be expected based on the incident laser pulse energy and previously measured absorption cross sections for the nanoplatelets. The reason for the discrepancy is not yet clear, but it most likely due to a fast decay or trapping process that is not captured within the time resolution of our time-resolved PL measurements; determining the mechanism behind these “lost excitons” will be the subject of future work.

With this calibration, we can determine the Auger recombination rate from the dynamics of $N(t)$. We approximate $N(t)$ as a continuous variable, and we consider only biexcitonic Auger recombination, ignoring both single-exciton recombination and processes that involve free carriers, such as trapping. We further assume that the rate of biexcitonic

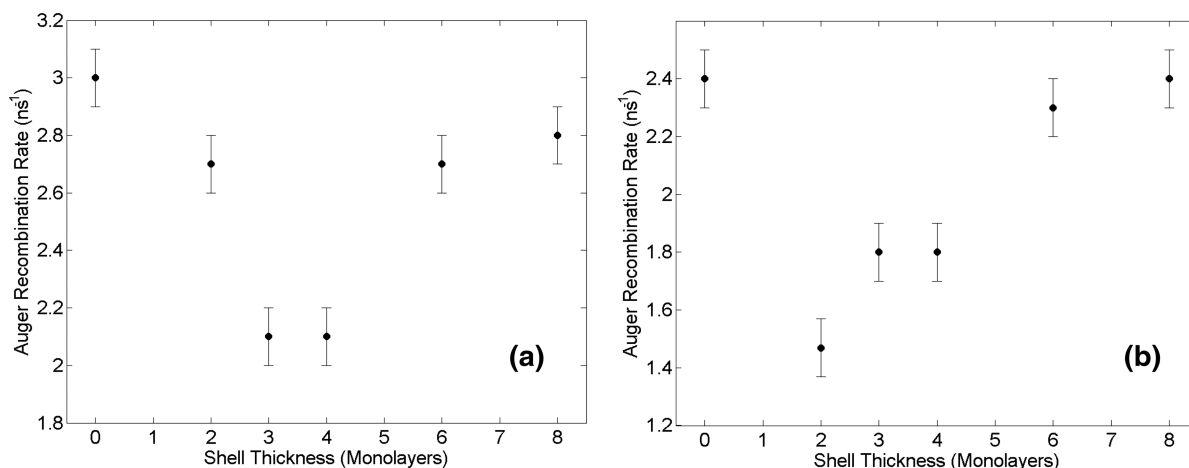


Figure 3. Auger recombination rate, A , as defined in the text, as a function of shell thickness for CdSe/CdS core/shell nanoplatelets with core thicknesses of (a) four monolayers and (b) five monolayers. Error estimates are based on the fitting error in the data analysis described in the text.

Auger recombination is proportional to the square of the exciton number. These approximations will hold only for $N(t) > 2$, corresponding to the initial part of the decay curve (in Figure 2b, for $t < 150$ ps). For lower values of $N(t)$, it would be necessary to include single-exciton recombination dynamics and trapping processes, and it will also be necessary to treat $N(t)$ as a discrete stochastic variable;³³ this will be the subject of future work.

Within the scope of these approximations, we can write

$$\frac{dN(t)}{dt} = -AN(t)^2 \quad (1)$$

where A is a coefficient that determines the dynamics of Auger recombination. Here, we will call A the Auger recombination rate, keeping in mind that it is an approximation of the true Auger rate based on the simplifying assumptions we have made in modeling the recombination dynamics. In other words, A reduces to the Auger recombination rate in the limit that other recombination mechanisms can be neglected. This parameter is different from the conventional Auger coefficient, which describes the three-carrier process that dominates in bulk semiconductors and has units of cm^6/s (ref 34). In NPLs, Auger recombination involves two bound excitons; in addition, we describe the exciton population in terms of the number of excitons per nanoplatelet (rather than the exciton density), so A has the units of s^{-1} .

Solving eq 1 gives

$$N(t) = \frac{N(0)}{1 + AN(0)t} \quad (2)$$

$1/N(t)$ is thus expected to depend linearly on t . We perform a corresponding linear fit on the initial part of the decay curve for the highest pump fluence, up to the point where single-exciton dynamics begin to dominate. A representative result is shown in Figure 2b. The fit is seen to correspond well to the data in the multiexciton regime, validating the assumption that biexcitonic Auger recombination dominates for $N(t) > 2$.¹⁹

Figure 2d compares the dynamics in the multiexciton regime and the corresponding fits for two samples of NPLs with the same core thickness and different shell thicknesses; a clear change in the Auger decay rate can be seen. The Auger coefficients obtained from similar fits on NPL samples with different core and shell thicknesses are summarized in Figure 3.

For both 4-ML and 5-ML CdSe cores, the Auger coefficient initially decreases with increasing thickness of the CdS shell, reaches a minimum for a shell thickness between 2 and 4 ML, and then increases as the shell thickness increases further.

Unlike single-carrier and single-exciton processes such as trapping and nonradiative recombination, Auger recombination is not expected to be sensitive to surface and interface defects. In addition, the dependence of the Auger coefficient on shell thickness follows the same trend for two separate sets of samples with different CdSe core thicknesses. This indicates that the nonmonotonic dependence of the Auger dynamics on shell thicknesses is intrinsic to the NPL structure, rather than being related to the quality of our specific sets of samples.

To further rule out the possibility that sample-quality issues are playing a role, we extended the measurements of single-exciton decay dynamics to longer time delays after excitation using time-correlated single-photon counting (TCSPC). (Measurement details are given in the Supporting Information.) A representative result is shown in Figure 4a. The decay curve fits well to the sum of three decaying exponentials, consistent with previous reports for this range of delay times.^{35,36} The decay on these time scales is understood to arise from single-exciton recombination,³⁶ with the three different time constants corresponding either to different decay channels or different populations of NPLs in the ensemble. The decay rates obtained from triexponential fits are summarized for the different samples in Figure 4b–c. All of the decay rates decrease monotonically with increasing shell thickness. This can be understood as the result of reduced electron–hole overlap: the electron confinement energy is larger than the conduction-band offset between CdSe and CdS, so the electron wave function extends into the CdS shell; on the other hand, the hole confinement energy is small compared to the valence-band offset, so holes remain confined in the CdSe core.³⁷ A possible exception to this trend is an apparent slight increase in some of the decay rates for 8-ML shells, but this is clearly distinct from the dependence of the Auger rates on shell thickness. If the biexciton decay rates shown in Figure 3 were dominated by nonradiative or trapping processes, then the single-exciton rates would be, as well, and both rates would be expected to follow the same trend. Similarly, if the decay rates in Figure 3 were due to radiative biexcitonic recombination, then they would be expected to follow a

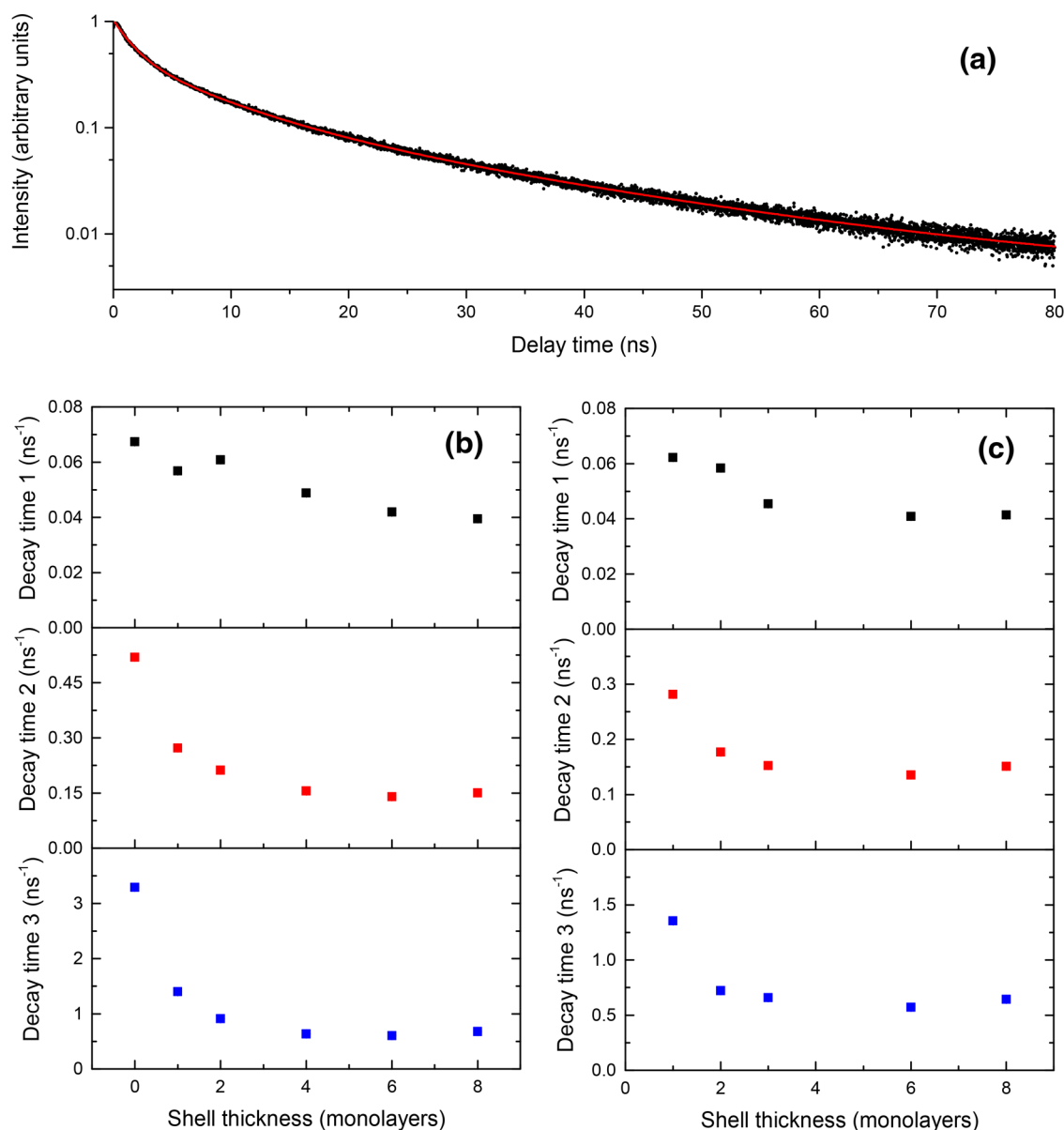


Figure 4. (a) Photoluminescence intensity from CdSe/CdS core/shell nanoplatelets (NPLs) with CdSe core thickness of 4 monolayers (ML) and CdS shell thickness of 4 ML as a function of time after pulsed excitation, for low excitation-pulse fluence and for long delay times. Black points are data; the red line is a fit to a triexponential decay. (b) Decay rates from triexponential fits of low-fluence photoluminescence intensity for CdSe/CdS core/shell NPLs with core thicknesses of 4 ML. (c) Decay rates for NPLs with core thicknesses of 5 ML.

trend similar to the single-exciton rates. The results thus indicate that the measured rates are indeed Auger recombination rates and that their dependence on shell thickness is a consequence of the electronic structure of the core/shell NPLs rather than defects or surface traps.

A previous study has observed a minimum in the Auger recombination rate of negatively charged trions—but not biexcitons—in type-II CdTe/CdSe core/shell QDs as a function of shell thickness.³⁸ In this case, the nonmonotonic behavior was explained by noting that the minimum in the Auger recombination rate corresponded to a shell thickness for which the electron energy is at the bottom of the CdTe conduction band; at this point, the electron Bloch function has zero p-orbital component, and the Auger matrix element goes to zero. This mechanism applies only to type-II heterostructures and thus does not play a role in CdSe/CdS core/shell nanocrystals.

On the other hand, a nonmonotonic dependence of the Auger rate on core and shell diameter has been predicted theoretically for type-I CdSe/CdS core/shell QDs.^{39,40} According to this model, the dominant process in biexcitonic Auger recombination involves the recombination of one exciton and the excitation of the electron in the other exciton from its ground state to a higher-lying state. The Auger recombination rate can be understood as depending primarily on the overlap integral between the initial and final electron wave functions in the second exciton; oscillations in this overlap with increasing shell size are responsible for oscillations in the Auger rate.

These predicted oscillations have not been observed experimentally for QDs, but this can be explained by inhomogeneous broadening in the QD ensembles that have been studied: since the calculated Auger rates are sensitive to small changes in the QD dimensions, and since there is a significant variance in QD diameter and shape in any ensemble,

the oscillations are averaged out. In NPL samples, by contrast, all the particles have the same thickness, so this averaging does not occur, and the intrinsic dependence of Auger rate on shell thickness is uncovered.

In summary, we have observed a nonmonotonic dependence of the Auger recombination rate in colloidal core/shell quantum wells on the shell thickness. Other NPL core/shell heterostructures made of different materials^{30,41} or with different electronic structures may provide additional control over Auger rates. For example, reduced Auger recombination rates have been observed for core/shell QDs with graded interfaces.^{22,24,42} A similar approach may enable a further reduction of Auger recombination in core/shell NPLs, leading to lower thresholds for gain and lasing, and enabling other optoelectronic applications, such as light-emitting diodes that do not suffer from efficiency droop at high powers.⁴³ Another important future direction will be to reconcile the current results, which imply a nonradiative biexciton Auger recombination rate significantly faster than the single-exciton radiative recombination rate, with a very recent report of nearly unity photoluminescence quantum yield for biexcitons in nanoplatelets.⁴⁴

■ ASSOCIATED CONTENT

■ Supporting Information

The Supporting Information is available free of charge on the ACS Publications website at DOI: 10.1021/acs.nanolett.7b03294.

Synthesis of nanoplatelets, optical measurements (PDF)

■ AUTHOR INFORMATION

ORCID

Matthew Pelton: 0000-0002-6370-8765

Dmitri V. Talapin: 0000-0002-6414-8587

Present Address

(I.F.): Chemistry Division, Los Alamos National Laboratory, Los Alamos, New Mexico 87545, U.S.A.

Author Contributions

M.P. conceived the experiment, performed streak-camera measurements, supervised TCSPC measurements, and prepared the manuscript. J.A. analyzed the data. I.F. synthesized nanoplatelet samples. D.T. supervised nanoplatelet synthesis. H.L. performed TCSPC measurements. S.O. and M.P. supervised data analysis. All authors contributed to discussions.

Notes

The authors declare no competing financial interest.

■ ACKNOWLEDGMENTS

We thank Richard Schaller for assistance with the streak-camera measurements, Arnaud Demortière for cross-sectional TEM imaging, and Alexander Efros for helpful discussions. This work was performed, in part, at the Center for Nanoscale Materials, a U.S. Department of Energy Office of Science User Facility under contract no. DE-AC02-06CH11357. Work at The University of British Columbia was funded by the Natural Sciences and Engineering Research Council of Canada. I.F. and D.V.T. acknowledge support from the National Science Foundation under award CHE-1611331. This work was partially supported by the University of Chicago Materials Research Science and Engineering Center, which is funded by

the National Science Foundation under award number DMR-1420709.

■ REFERENCES

- (1) Ithurria, S.; Dubertret, B. *J. Am. Chem. Soc.* **2008**, *130*, 16504–16505.
- (2) Ithurria, S.; Tessier, M. D.; Mahler, B.; Lobo, R. P. S. M.; Dubertret, B.; Efros, A. L. *Nat. Mater.* **2011**, *10*, 936–941.
- (3) She, C.; Fedin, I.; Dolzhenkov, D. S.; Demortière, A.; Schaller, R. D.; Pelton, M.; Talapin, D. V. *Nano Lett.* **2014**, *14*, 2772–2777.
- (4) Guzelturk, B.; Kelestemur, Y.; Olutas, M.; Delikanli, S.; Demir, H. V. *ACS Nano* **2014**, *8*, 6599–6605.
- (5) She, C.; Fedin, I.; Dolzhenkov, D. S.; Dahlberg, P. D.; Engel, G. S.; Schaller, R. D.; Talapin, D. V. *ACS Nano* **2015**, *9*, 9475–9485.
- (6) Diroll, B. T.; Talapin, D. V.; Schaller, R. D. *ACS Photonics* **2017**, *4*, 576–583.
- (7) Li, M.; Zhi, M.; Zhu, H.; Wu, W.-Y.; Xu, Q.-H.; Jhon, M. H.; Chan, Y. *Nat. Commun.* **2015**, *6*, 8513.
- (8) Olutas, M.; Guzelturk, B.; Kelestemur, Y.; Yeltik, A.; Delikanli, S.; Demir, H. V. *ACS Nano* **2015**, *9*, 5041–5050.
- (9) Grim, J. Q.; Christodoulou, S.; Di Stasio, F.; Krahne, R.; Cingolani, R.; Manna, L.; Moreels, I. *Nat. Nanotechnol.* **2014**, *9*, 891–895.
- (10) Yang, Z.; Pelton, M.; Fedin, I.; Talapin, D. V.; Waks, E. *Nat. Commun.* **2017**, *8*, 143.
- (11) Klimov, V. I.; Mikhailovsky, A. A.; McBranch, D. W.; Leatherdale, C. A.; Bawendi, M. G. *Science* **2000**, *287*, 1011–1013.
- (12) Klimov, V. I. *Annu. Rev. Condens. Matter Phys.* **2014**, *5*, 285–316.
- (13) Klimov, V. I.; Mikhailovsky, A. A.; Xu, S.; Malko, A.; Hollingsworth, J. A.; Leatherdale, C. A.; Eisler, H.-J.; Bawendi, M. G. *Science* **2000**, *290*, 314–317.
- (14) Eisler, H.-J.; Sundar, V. C.; Bawendi, M. G.; Walsh, M.; Smith, H. I.; Klimov, V. *Appl. Phys. Lett.* **2002**, *80*, 4614–4616.
- (15) Klimov, V. I.; Ivanov, S. A.; Nanda, J.; Achermann, A.; Bezel, I.; McGuire, J. A.; Piryatinski, A. *Nature* **2007**, *447*, 441–446.
- (16) García-Santamaría, F.; Chen, Y.; Vela, J.; Schaller, R. D.; Hollingsworth, J. A.; Klimov, V. I. *Nano Lett.* **2009**, *9*, 3482–3488.
- (17) Dang, C.; Lee, J.; Breen, C.; Steckel, J. S.; Coe-Sullivan, S.; Nurmikko, A. *Nat. Nanotechnol.* **2012**, *7*, 335–339.
- (18) Grivas, C.; Li, C.; Andreakou, P.; Wang, P.; Ding, M.; Brambilla, G.; Manna, L.; Lagoudakis, P. *Nat. Commun.* **2013**, *4*, 2376.
- (19) Kunneman, L. T.; Tessier, M. D.; Heuclin, H.; Dubertret, B.; Aulin, Y. V.; Grozema, F. C.; Schins, J. M.; Siebbeles, L. D. A. *J. Phys. Chem. Lett.* **2013**, *4*, 3574–3578.
- (20) Baghani, E.; O'Leary, S. K.; Fedin, I.; Talapin, D. V.; Pelton, M. *J. Phys. Chem. Lett.* **2015**, *6*, 1032–1036.
- (21) Li, Q.; Lian, T. *Nano Lett.* **2017**, *17*, 3152–3158.
- (22) García-Santamaría, F.; Brovelli, S.; Viswanatha, R.; Hollingsworth, J. A.; Htoon, H.; Crooker, S. A.; Klimov, V. I. *Nano Lett.* **2011**, *11*, 687–693.
- (23) Chen, Y.; Vela, J.; Htoon, H.; Casson, J. L.; Werder, D. J.; Bussian, D. A.; Klimov, V. I.; Hollingsworth, J. A. *J. Am. Chem. Soc.* **2008**, *130*, 5026–5027.
- (24) Nasilowski, M.; Spinicelli, P.; Patriarche, G.; Dubertret, B. *Nano Lett.* **2015**, *15*, 3953–3958.
- (25) Zavelani-Rossi, M.; Lupo, M. G.; Tassone, F.; Manna, L.; Lanzani, G. *Nano Lett.* **2010**, *10*, 3142–3150.
- (26) Rabou, F. T.; Lunnemann, P.; van Dijk-Moes, R. J. A.; Frimmer, M.; Pietra, F.; Koenderink, A. F.; Vanmaekelbergh, D. *Nano Lett.* **2013**, *13*, 4884–4892.
- (27) Ithurria, S.; Talapin, D. V. *J. Am. Chem. Soc.* **2012**, *134*, 18585–18590.
- (28) Mahler, B.; Nadal, B.; Bouet, C.; Patriarche, G.; Dubertret, B. *J. Am. Chem. Soc.* **2012**, *134*, 18591–18598.
- (29) Tessier, M. D.; Javaux, C.; Maksimovic, I.; Lorient, V.; Dubertret, B. *ACS Nano* **2012**, *6*, 6751–6758.

- (30) Riedinger, A.; Ott, F. D.; Mule, A.; Mazzotti, S.; Knüsel, P. N.; Kress, S. J. P.; Prins, F.; Erwin, S. C.; Norris, D. J. *Nat. Mater.* **2017**, *16*, 743–748.
- (31) Pelton, M.; Ithurria, S.; Schaller, R. D.; Dolzhenkov, D. S.; Talapin, D. V. *Nano Lett.* **2012**, *12*, 6158–6163.
- (32) Achtstein, A. W.; Schliwa, A.; Prudnikau, A.; Hardzei, M.; Artemyev, M. V.; Thomsen, C.; Woggon, U. *Nano Lett.* **2012**, *12*, 3151–3157.
- (33) Barzykin, A. V.; Tachiya, M. J. *Phys.: Condens. Matter* **2007**, *19*, 065105.
- (34) Chen, S. L. *Physics of Photonic Devices*, 2nd ed.; Wiley: Hoboken, NJ, 2009.
- (35) Kunneman, L. T.; Schins, J. M.; Pedetti, S.; Heuclin, H.; Grozema, F. C.; Houtepen, A. J.; Dubertret, B.; Siebbeles, L. D. A. *Nano Lett.* **2014**, *14*, 7039–7045.
- (36) Olutas, M.; Guzelturk, B.; Kelestemur, Y.; Yeltik, A.; Delikanli, S.; Demir, H. M. *ACS Nano* **2015**, *9*, 5041–5050.
- (37) Sitt, A.; Della Sala, F.; Menagen, G.; Banin, U. *Nano Lett.* **2009**, *9*, 3470–3476.
- (38) Qin, W.; Liu, H.; Guyot-Sionnest, P. *ACS Nano* **2014**, *8*, 283–291.
- (39) Vaxenburg, R.; Rodina, A.; Lifshitz, E.; Efros, A. L. *Nano Lett.* **2016**, *16*, 2503–2511.
- (40) Jain, A.; Voznyy, O.; Hoogland, S.; Korkusinski, M.; Hawrylak, P.; Sargent, E. H. *Nano Lett.* **2016**, *16*, 6491–6496.
- (41) Lhuillier, E.; Pedetti, S.; Ithurria, S.; Nadal, B.; Heuclin, H.; Dubertret, B. *Acc. Chem. Res.* **2015**, *48*, 22–30.
- (42) Cragg, G. E.; Efros, A. L. *Nano Lett.* **2010**, *10*, 313–317.
- (43) Bae, W. K.; Park, Y.-S.; Lim, J.; Lee, D.; Padilha, L. A.; McDaniel, H.; Robel, I.; Lee, C.; Pietryga, J.; Klimov, V. *Nat. Commun.* **2013**, *4*, 2661.
- (44) Ma, X.; Diroll, B. T.; Cho, W.; Fedin, I.; Schaller, R. D.; Talapin, D. V.; Gray, S. K.; Wiederrecht, G. P.; Gosztola, D. J. *ACS Nano* **2017**, *11*, 9119–9127.